The Interaction Between Dynamics and Chemistry of Ozone in the Set-up Phase of the Northern Hemisphere Polar Vortex

S. R. Kawa[1], R. Bevilacqua[2], J. J. Margitan[3], A. R. Douglass[1], M. R. Schoeberl[1], K. Hoppel[2], B. Sen[3]

[1]NASA Goddard Space Flight Center, Greenbelt, Maryland

[2]Naval Research Laboratory, Washington, DC

[3]Jet Propulsion Laboratory, California Institute of Technology, Pasadena, California

Submitted to the Journal of Geophysical Research

November 13, 2001

ABSTRACT

The morphology and evolution of the stratospheric ozone (O_3) distribution at high latitudes in the Northern Hemisphere (NH) are examined for the late summer and fall seasons of 1999. This time period sets the O_3 initial condition for the SOLVE/THESEO field mission performed during winter 1999-2000. In situ and satellite data are used along with a three-dimensional model of chemistry and transport (CTM) to determine the key processes that control the distribution of O_3 in the lower-to-middle stratosphere. O_3 in the vortex at the beginning of the winter season is found to be nearly constant from 500 to above 800 K with a value at 3 ppmv +/- ~10%. Values outside the vortex are up to a factor of 2 higher and increase significantly with potential temperature. The seasonal time series of data from POAM shows that relatively low O_3 mixing ratios, which characterize the vortex in late fall, are already present at high latitudes at the end of summer before the vortex circulation sets up. Analysis of the CTM output shows that the minimum O_3 and increase in variance in late summer are the result of 1) stirring of polar concentric O_3 gradients by nascent wave-driven transport, and 2) an acceleration of net photochemical loss with decreasing solar illumination. The segregation of low O_3 mixing ratios into the vortex as the circulation strengthens through the fall suggests a possible feedback role between O_3 chemistry and the vortex formation dynamics. Trajectory calculations from O_3 sample points early in the fall, however, show only a weak correlation between initial O_3 mixing ratio and potential vorticity later in the season consistent with order-of-magnitude calculations for the relative importance of O_3 in the fall radiative balance at high latitudes. The possible connection between O_3 chemistry and the dynamics of vortex formation does suggest that these feedbacks and sensitivities need to be better understood in order to make confident predictions of the recovery of NH O_3.

1. INTRODUCTION

The future of stratospheric O_3, especially in the Northern Hemisphere (NH) polar region, is uncertain. Decreasing abundances of reactive chlorine in the stratosphere [J. W. Elkins, personal communication, 2001], resulting from international regulation of chlorofluorocarbon emissions, should result in a recovery of polar O_3 toward its pre-industrial levels [WMO, 1999]. On the other hand, the consequences of increasing greenhouse gases and global warming in the lower atmosphere will most likely lead to conditions more conducive to O_3 destruction, i.e., colder polar stratospheric temperatures, increased stratospheric water vapor, or altered wave driving [Fels et al., 1980; Kirk-Davidoff et al., 1999; Shindell et al., 1999]. These changes lead to increased probability of polar stratospheric cloud (PSC) formation, enhanced activation of reactive chlorine, and accelerated O_3 loss. Total O_3 at high latitudes in March, when chlorine-induced O_3 loss is generally at its maximum in the NH, shows evidence of a 10-year decreasing trend in 1988-1997; however 3 of the past 4 years including 2001 show relatively high O_3, similar to levels before 1990 [Newman and Harris, 2002]. We need to better understand the chemical and dynamical processes that produce the observed changes in polar O_3 in order to predict the future of stratospheric O_3 with confidence in the face of changing climate and trace gas abundances.

Springtime O_3, particularly in the lower stratospheric polar vortex, is controlled by vertical and horizontal transport, and chemical loss through the winter and spring. Vortex O_3 in spring also depends somewhat on the initial O_3 present in fall season when the vortex forms. Accurate knowledge of the initial vortex O_3 distribution is needed to diagnose O_3 chemical and dynamic

changes that occur over the course of the winter and spring [e.g., Manney et al., 1994; Mueller et al., 1997].

The need to better understand the details of NH polar O_3 change motivated the SAGE III Ozone Loss and Validation Experiment/Third European Stratospheric Experiment on Ozone 2000 (SOLVE/THESEO) [Newman and Harris, 2002], which was conducted during the 1999-2000 NH winter. The present study is set in the SOLVE/THESEO context to provide a good characterization of the initial condition against which the contributions of O_3 chemical and transport changes can be evaluated for the winter and spring 1999-2000, and to examine the processes that produce the initial O_3 distributions as the vortex forms.

Previous studies of stratospheric vortex formation have established that the early development is controlled primarily by the seasonal progression of zonally symmetric net radiative heating and cooling, which produces initial temperature decrease, descent, and strong cyclonic circulation [Butchart and Remsberg, 1986; O'Neill and Pope, 1990; Schoeberl and Hartmann, 1991]. Later in the fall season, planetary wave propagation becomes relatively more important in determining the temperature, descent rate, and size and position of the vortex [Clough et al., 1985; Juckes and O'Neill, 1988]. Evidence for these processes has been derived from analysis of trace gas observations as well as meteorological fields [e.g., Butchart and Remsberg, 1986; Ruth et al., 1994; Manney et al., 2000]. Vortex climatologies [Baldwin and Holton, 1988; Waugh and Randel, 1999] show that the vortex develops similarly in each hemisphere and that there is only a small degree of interannual variability in the early months (October-November in the NH). The observed hemispheric and interannual similarity supports the primary role of net radiative

cooling in vortex formation. The radiative balance in the polar stratosphere is predominantly between cooling from CO2 emission and absorption of sunlight by O_3. Emission by water vapor and O_3 makes a contribution of less than 10% [Rosenfield, 1992].

While numerous studies have addressed the details of the processes that control vortex maintenance during winter and its dissipation in stratospheric warmings, comparatively little work has been done on the details of vortex formation and, in particular, the evolution of O_3 during vortex formation. We are interested in the fall O_3 distribution for several reasons. As mentioned above, the initial winter distribution of O_3 must be well characterized in order to distinguish the effects of chemical and transport processes through the winter. More generally, we need to understand the details of the processes that control the seasonal cycle of O_3 through the fall in order to interpret observed variability. Finally, since O_3 is the primary absorber on the solar heating side of the net radiation balance, its distribution must play a role in the dynamics of vortex development. This raises the possibility of coupling and feedbacks between the chemical, radiative, and dynamical processes that are not fully implemented in most numerical models.

Leovy et al. [1985] showed that O_3 from LIMS in the NH middle stratosphere at 10 mbar in the October 29 vortex was zonally symmetric with a deep minimum (<3 ppmv) at the pole, which they initially termed an "ozone hole." The zonal symmetry was perturbed through November and only weak gradients inside the vortex are evident in December [Leovy et al., 1985; Butchart and Remsberg, 1986]. Perliski et al. [1989] directly address the seasonal cycle of O_3 at high latitudes in comparison to SBUV data in a 2-D model; however, the polar vortex is not well represented in the 2-D context. O_3 and other trace gas distributions from ATMOS in the early

vortex were analyzed for their transport characteristics by Manney et al. [1999], but these data are available only at the edge of the developing vortex with no sampling at high equivalent latitudes. Little analysis has been done on the characteristics and causes of the O_3 distribution in the developing vortex.

In this paper we analyze in situ and satellite data along with output from a three-dimensional (3D) chemistry and transport model (CTM), which uses winds and temperatures from meteorological data assimilation (Douglass et al. [2001] and references within). Detailed analysis of the evolution of O_3 at high latitudes is enabled by data from the Polar Ozone and Aerosol Measurement III (POAM III) satellite instrument. The POAM III data is also anchored by in situ O_3 data from the Observations of the Middle Stratosphere (OMS) balloon platform, which has very high vertical resolution and absolute accuracy.

POAM III is a visible/near infrared photometer (similar to the SAGE II instrument) for making measurements of ozone, aerosol extinction, water vapor, and nitrogen dioxide in the polar stratosphere using the solar occultation technique [Lucke et al., 1999]. POAM III makes 14-15 measurements per day in each hemisphere around a circle of latitude, with a longitudinal spacing of about 25 degrees. The measurement latitude varies slowly over the year. In the northern hemisphere the annual latitudinal measurement range is 55° N to 73° N, and the measurement coverage exhibits nearly exact annual periodicity (a graphical representation of the POAM measurement coverage is given by Lumpe et al. [2002]). In this study, we use version 3 POAM III ozone retrievals, which have a vertical resolution of about 1.1 km, and random error levels of < 10% above 10 km (< 5% above 15 km) [Lumpe et al., 2001]. The POAM III ozone retrievals

have been validated by comparison with O_3 sonde and satellite measurements by Rusch et al. [2002], and detailed comparisons to other ozone measurements made during the SOLVE campaign are given by Lumpe et al. [2002].

The purpose of this paper is two-fold. The first is simply to characterize the O_3 initial distribution for the SOLVE/THESEO period. This analysis will facilitate interpretation of O_3 loss calculations through the SOLVE/THESEO winter and has implications for derivation of O_3 loss in other years as well. The O_3 distribution turns out to have very interesting morphological features related to the vortex dynamical structure and to high-latitude chemistry. This leads to the second objective, which is to examine how the initial winter O_3 distribution evolves through a combination of chemistry and transport processes. This in turn leads us to begin to explore the extent to which the O_3 distribution may exert control on vortex circulation development, which holds inferences about potential O_3/dynamical feedbacks.

2. OBSERVATIONS OF INITIAL VORTEX O_3

We take late November as our starting point in time for the vortex initial O_3. By late November the vortex circulation is well established (Figure 1) but temperatures have not yet been widely or consistently cold enough in the lower stratosphere [Manney and Sabutis, 2000; Newman and Harris, 2002] for PSC formation and chlorine activation. The largest springtime O_3 decreases observed in the NH vortex take place in the lower stratosphere at potential temperatures of about 450 to 500 K in March [Sinnhuber et al., 2000; Richard et al. 2001; Rex et al., 2002; Schoeberl et al., 2002; Salawitch et al. 2002]. Air at these altitudes in March 2000 originated in the vortex

in November 1999 at about 530 to 600 K based on diabatic trajectory calculations [Schoeberl et al., 2002] and changes in tracer gradients [Ray et al. 2002]. Thus the potential temperature region of primary interest for this study is around 500 to 800 K.

The O_3 profile measured from the OMS in situ balloon payload [Salawitch et al., 2002 and references within] launched from Esrange, Sweden (68° N, 21° E) on November 19, 1999 is shown in Figure 1. The O_3 mixing ratio is near 3 (+/- 0.5) ppmv from below 500 K up to the highest measurement point near 900 K. Also shown in Figure 1 are profiles from POAM at nearby locations, which were taken two days previous and one day after the OMS profile. POAM O_3 profiles are not available near the OMS location on Nov. 18 or 19 due to safety precautions for the Leonid meteor shower. The profile on Nov. 17 is somewhat closer to the vortex edge (lower potential vorticity (PV)) than those shown for OMS on Nov. 19 and POAM on Nov. 20. The POAM profile for Nov 20 is similar to the OMS profile within 10% (see also Lumpe et al. [2002]). This lends important confidence to the quality of both data sets. The stated accuracy of the OMS O_3 instrument is 3-5% and the POAM O_3 is <10% [Salawitch et al., 2002; Lumpe et al., 2002]. The MkIV instrument [Toon et al., 1999] is also within 10% of the POAM III data from a balloon flight in the vortex on December 3, 1999 [Lumpe et al., 2002].

Also shown in Figure 1 is the profile from a climatology of O_3 for November at 65° N based on O_3 sonde and SAGE II data [Logan and McPeters, 1999]. Clearly the zonal mean, monthly average climatology is not a good description of the measured vortex ozone in Figure 1.

Figure 2 shows the set of NH ozone profiles measured by POAM on November 30, 1999 color-coded by PV at 650 K. November 30 is shown as an example day with good PV coverage; other days in late November are similar. Those profiles inside the polar vortex have a characteristic distribution similar to that seen in Figure 1, a very small vertical gradient and a mixing ratio near 3 ppmv. The profiles from outside the vortex have higher mixing ratios and a stronger altitude gradient. Figure 2 also suggests that the climatological O_3 profile from Figure 1 represents an average of profiles inside and outside the vortex along the same latitude. The observed displacement of the vortex from the pole and the position of the Aleutian high are common features in the fall, sometimes referred to as a Canadian warming [Labitzke, 1977; 1982].

Figure 3 shows the equivalent latitude-potential temperature average of POAM O_3 for the second half of November 1999. This plot confirms that the characteristic O_3 profile distributions seen in Figures 1 and 2 are consistent throughout the time period across many POAM samples. Subsequent sections of this paper explore how stratospheric chemistry and dynamics combine to produce the initial vortex O_3 distribution summarized in these figures.

One feature that is not fully consistent with our characterization of nearly constant vortex O_3 at a mixing ratio of 3 ppmv is the 'notch' in the OMS profile near 550 K, which has a mixing ratio minimum of 2.4 ppmv (Figure 1, and also discussed by Salawitch et al. [2002]). This feature is not seen in the corresponding POAM data. The POAM vertical resolution for O_3 in this altitude range is about 1.1 km [Lucke et al., 1999] so POAM should be expected to resolve this feature, which has a vertical depth of about 3 km. Two questions then arise, is vortex air with mixing ratios near 2.5 ppmv more commonplace than the analysis above would indicate, and what led to

the relatively lower O_3 seen in this measurement? POAM does occasionally measure O_3 less than 3 ppmv at 550 to 600 K, and this appears as slightly higher standard deviation in Figure 3. However the number of POAM profiles with O_3 less than 2.7 ppmv in November is small (3) and the mean is still 3 +/- 0.3 ppmv in the region of interest. Examination of 15 O_3 sonde profiles from Nye Alesund (79° N, 12° E) in November and December 1999 finds one other profile (Nov 11) with a similar low O_3 "notch," with 2.7 ppmv at 22 mbar. The preponderance of the sonde profiles looks very similar to those from POAM in Figure 2. Note also that the OMS Mk IV O_3 profile on December 3, 1999 from Esrange does not have the low O_3 feature and is very similar to the corresponding POAM profile. Thus we conclude that vortex air with mixing ratios significantly less than 3 ppmv is uncommon in this time period. The origin of the notch feature appears to be a remnant of low O_3 produced earlier in the fall that has not been well mixed in the vortex. Note that the nitric acid trihydrate (NAT) condensation temperature is about 191 K at 20 mbar increasing to 195 K at 50 mbar with 5 ppmv H2O and typical amounts of HNO_3: 10 and 6 ppmv, respectively. Minimum analyzed temperatures were not below the NAT condensation temperature by the time of the OMS flight [Manney and Sabutis, 2000; Newman and Harris, 2002], and there is no indication of early-season, accelerated O_3 chemical loss [Salawitch et al., 2002].

3. EVOLUTION OF O_3 IN THE FALL SEASON

Figure 4 shows POAM O_3 profiles in mid-September, 1999, before the vortex has begun to spin up. Although the high-latitude O_3 data for this time of year show a relatively large degree of variability (similar to the range in Figure 4), the characteristics are clearly quite different from

the November profiles (Figure 2). In September the O_3 amount generally increases with altitude and mixing ratios range from about 2.5 to 6 ppmv over 500 to 900 K. The PV gradient is small at this time. Diabatic back trajectories indicate that air in the vortex at 650 K at the end of November descends from about 720 K at high latitudes in mid-September (Section 5).

The complete POAM III time series (Figure 5) shows regularly repeating features in the seasonal evolution of O_3 at 650 K. Through late spring and summer, O_3 has relatively low variance and steadily declining mixing ratios. In late summer we see a sharp increase in variance and the appearance of minimum mixing ratios near the equinox. Minimum O_3 mixing ratios are as low as 2.2 ppmv. Variance is high through the fall and mixing ratios increase overall. Data at 650 K are shown since this potential temperature is near the middle of the range of interest. Similar characteristics are seen at 600, 720, and 800 K, however 500 K is quite different [Hoppel et al., 1999]. At 500 K minimum O_3 mixing ratios occur near August 1 with low variance ($\pm$10%), and then increase to a Jan-Feb maximum. Variability in O_3 at 500 K increases later in the fall with the strengthening and distortion of the vortex, consistent with transport dominated changes. Note that the POAM sampling is modulated by changing latitude. From mid August through November, 1999 the POAM sampling latitude is between 60 and 71° N.

Figure 6 shows a close up of the O_3 data for 1999 with points color coded by PV. The clear segregation of lower O_3 in the vortex, seen in Figure 2, is also apparent in Figure 6. Figure 6 makes clear that mixing ratios less than 3.3 ppmv, typical of the November vortex, are already present at the end of the summer at high latitudes. There is no need to invoke deep descent in the vortex, for example, to explain the relatively low mixing ratios there. Although low O_3 mixing

ratio values in September are not necessarily connected to the vortex air in November, Figure 6 raises the interesting possibility of a mechanistic link between the evolution of O_3 at high latitudes and development of the polar vortex that will be explored further.

4. DEVELOPMENT OF LOW O_3 MIXING RATIOS

In this section we use output from the Goddard 3-D CTM to diagnose the mechanisms behind the development of low O_3 mixing ratios seen in late summer through fall in Figures 3 through 6.

The CTM used here is an improved version of that used in previous analyses of observations from the Halogen Occultation Experiment [Douglass and Kawa, 1997] and from POAM, ozonesondes, and a lidar on the NASA DC-8 [Douglass et al., 2001]. Winds and temperatures are taken from the version of the Goddard Earth Observing System Data Assimilation that was in operational use during the SOLVE mission. The horizontal resolution of the assimilation fields is 1° by 1°, and the stratospheric fields are noisier than those produced by prior assimilation systems that utilized a 2° latitude by 2.5° longitude horizontal grid. The vertical winds are calculated to maintain continuity, and the noisy horizontal winds lead to extremely noisy vertical winds. To ameliorate the problems in the stratospheric transport caused by this non-physical noise, the horizontal winds are smoothed, mapped to a coarser grid of 2° by 2.5°, and smoothed again before being used to calculate constituent transport.

The transport and photochemical contributions to the constituent continuity equations are solved sequentially. Advection utilizes the scheme developed by Lin and Rood [1996]; this scheme

maintains sharp gradients and appropriate correlations for long-lived constituents, and does not produce unrealistic maxima or minima. The photochemical scheme includes all gas phase reactions thought to be important in the stratosphere. Rate constants are taken from JPL [1997] with modifications to NOx/NOy rates consistent with JPL [2000]. The same schemes described by Douglass and Kawa (1999) are used for particle growth and formation and to determine the rates of heterogeneous reactions. Photolysis rates are calculated using temperature dependent cross sections and attenuated solar fluxes that are interpolated from a table lookup based on the model of Anderson and Lloyd [1990]. These photolysis rates compare favorably with the photolysis benchmark that was developed as part of the Atmospheric Effects of Aviation Project [Stolarski et al., 1995]. The simulation is initialized using the results of a simulation that was driven by winds and temperatures from the previous version of the assimilation system.

The CTM O_3 time series (Figure 7) and profiles (not shown) show the same key features as the POAM data, although with some mixing ratio offset. We use the CTM to examine the chemical and transport mechanisms behind the observed behavior. In addition, the CTM is able to fill in the limited POAM latitude sampling. The development of minimum mixing ratios and increased variance, characteristic of the data in early September, is seen at latitudes from 62 to 82° N in the CTM at 650 K. This suggests that the POAM observed O_3 changes in Figure 6 are not the result of aliasing a latitude gradient into the time series by changing sample latitude. At 800 K, the minimum mixing ratio occurs slightly later, near October 10, consistent with the POAM data. The distributions seen in Figures 6 and 7 are similar at potential temperatures from 600 to 800 K and the time series changes do not represent a simple descent of air across isentropes through the time period.

The seasonal decrease in lower stratospheric O_3 at mid to high latitudes through the summer is a climatological feature of the O_3 seasonal cycle [Bowman and Krueger, 1985]. This seasonal decline was the subject of intense scrutiny during the POLARIS field campaign [Newman et al., 1999]. The summertime decrease is usually attributed to photochemical loss processes, which exceed production and resupply of O_3 via transport from higher altitudes and lower latitudes [Fahey and Ravishankara, 1999; Bruhl and Crutzen, 2000]. In mid summer, in situ production and loss are large in the high sun conditions, and wave driven transport is at a minimum [Perliski et al., 1989]. Summertime transport of O_3 is generally considered to be small compared to chemistry, although transport may also play a role in the seasonal decline [Rosenlof, 1999; Cordero and Kawa, 2001].

Examination of the CTM output demonstrates how two factors combine to produce the observed high variance and minimum O_3 values in late summer. The increase in variance is the result of stirring the circumpolar O_3 gradients at the end of summer as the wave activity begins to increase (Figure 8). Asymmetric wave motions bring higher O_3 from lower latitudes poleward and push low O_3 near the pole out to the latitudes near 68° sampled by POAM (see also Park and Russell [1994]; Bruhl et al. [1998]). In addition, the high latitude net O_3 photochemical loss is accelerated at this time. Figure 9 shows that the net O_3 percentage loss from the CTM at high latitudes maximizes in late summer. Both production and loss maximize at the summer solstice and the terms are near photochemical balance through September 1 at 66 to 70° N, 650 K. As the solar zenith angles increase, O_3 production from O2 photolysis falls off faster than O_3 loss from radical catalytic cycles (see also Perliski et al. [1989] and Farman et al. [1985]). This

happens because O2 photolysis occurs at shorter wavelengths, which are attenuated more at moderate zenith angles, than photolysis of the radical intermediates in O_3 loss. As a result, air parcels whose trajectory paths are confined to high latitudes lose O_3 relatively quickly. The latitude of maximum loss moves equatorward through the fall and all photochemical activity ceases when the sun leaves the high latitudes for the season. Larger percentage losses are seen at higher altitudes, which tends to flatten the vertical O_3 gradient as observed.

As the vortex strengthens through October, the isentropic minimum values increase slightly consistent with continued mixing, which dilutes the minima (in the CTM at least), and increased diabatic descent, which tends to increase O_3 in the vortex (Figures 6, 7, and 4). The low O_3 abundances, however, are largely maintained in the vortex, which is increasingly isolated from lower latitude, higher O_3 air, as the circulation increases. A strong O_3 gradient across the vortex edge in November is produced by transport and mixing of lower latitude to higher latitudes outside of the vortex (Figures 2, 6).

Back trajectory calculations from the POAM data points also substantiate that both accelerated photochemical loss and stirring are what drives the seasonal minimum O_3 mixing ratios seen in Figures 5 and 6. Trajectories from POAM sample locations near 68° N in mid-September going back to mid-August show that the parcels with the lowest O_3 mixing ratios in September are those with the least travel to lower latitudes and thus continuous exposure to conditions of maximum photochemical loss. That is, high average parcel latitude is well correlated with low O_3. However, high initial latitude on August 16 is not well correlated with low O_3 in September, which argues against simple passive transport as the dominant process. Although uncertainty in

trajectories may be significant, this suggests that continued photochemical loss is required in addition to stirring of the low polar O_3 created throughout summer, consistent with the analysis of Hoppel et al. [1999]. The minimum O_3 in the model and the data occurs at the autumnal equinox at 650 K and around October 10 at 800 K.

5. DYNAMICS OF VORTEX FORMATION

We turn now to the question of a possible mechanistic link between low O_3 values and the formation of the vortex, as suggested by Figure 6. The primary mechanism driving the formation of the polar winter vortex is radiative cooling at high latitudes, which dominates solar heating in low sun conditions. As the temperature cools, air descends and vorticity increases. This produces a relatively isolated vortex air mass with strong westerly winds. Longwave cooling clearly dominates the radiative forcing at high latitudes in fall, at least in the meteorological model underlying the CTM (Figure 10). More than 90% of this long wave cooling is due to CO2 and H2O emission. O_3 is only a minor contributor to the long wave cooling, but solar heating is due almost entirely to O_3 [Rosenfield, 1992]. Poleward of 60°N, shortwave heating from absorption by O_3 is about 20% of the net through October so a 50% variation in O_3 (e.g., Figure 6) would result in a 10% variation in net forcing. Thus, it is feasible that O_3 variations and their radiative forcing may exert some influence on vortex formation, although clearly they are not dominant. This effect at the 10% level may help to segregate low O_3 parcels into the vortex. We use trajectory calculations to see if we can estimate the effect of O_3 variations in vortex formation.

Back trajectories from November 30, when the vortex is fully developed, to September 15, when little PV gradient exists, show a surprising degree of organization (Figure 11). Figure 11d shows that the air which eventually becomes the vortex originates almost exclusively from latitudes north of 67° in mid-September. A few trajectories that start at high latitudes in September do not end up in the vortex, but most map into the vortex in November. The distribution of trajectory endpoints in September (Figure 11b) is fairly complete, i.e., there are no large areas in September that are not sampled by the back trajectories. Similar plots at different times along the back trajectories show that the correspondence between vortex and latitude greater than 65° is maintained from 75 through about 20 days back indicating that the air was continually located at high latitudes as the vortex developed. This is consistent with the time series of PV distributions. On about November 17, a wave-one warming developed and the vortex became asymmetric and shifted off the pole similar to the pattern seen in Figure 11a.

The high-latitude air descends from a 720 K starting point, but descent occurs on a wider spatial scale than the vortex (Figure 11c), consistent with a broad region of cooling. The descent in the vortex air, however, occurs earlier in time by about 15 days than that in the surrounding region, which catches up to the vortex over the last 15 days preceding November 30.

This trajectory analysis is consistent with previous studies cited above that emphasize the strong, zonally symmetric radiative forcing that drives the early formation of the vortex, and the transition to a more strongly wave-driven regime as the vortex circulation strengthens. It also demonstrates that our POAM samples of interest are taken near the edge (~67° N) of the source region for vortex air in September.

Whether the early fall O_3 variance exerts significant control on the vortex development is difficult to discern from the data. Forward trajectory calculations from 75 POAM points in mid September show only a weak correlation between initial O_3 and final PV or between initial O_3 and final potential temperature. A strong correlation might be expected if the low O_3 were in fact dominating control of which parcels became vortex air. A similar test with MLS O_3 [Froidevaux et al., 1994] for 1995, which has more complete latitude coverage (up to 80° N) in September, also does not show a strong correlation between low O_3 and PV or potential temperature. Comparing Figure 11b with Figure 8 suggests that perhaps the vortex parcels tend to originate preferentially from the lower O_3 quadrants in the September O_3 distribution (720 K is very similar to 650 K), but the trajectory correlations of CTM O_3 in mid September with PV on November 30 show a lot of scatter. The weak correlations may not be surprising in view of potential errors in long trajectory runs and the difficulty of diagnosing the effect of a relatively small perturbation to the total forcing.

6. CONCLUSIONS

The distribution of O_3 at high northern latitudes in the lower-to-middle stratosphere at the beginning of the winter season, 1999-2000, is found to have a characteristic distribution consistent between in situ and satellite measurements. Initial O_3 profiles in the vortex are similar to each other and are quite different from outside the vortex at the same latitude and also from a zonal mean climatology. In the vortex, O_3 is nearly constant from 500 to above 800 K with a

value at 3 ppmv +/- ~10%. Values outside the vortex are up to a factor of 2 higher and increase significantly with potential temperature.

The seasonal time series of POAM data shows that relatively low O_3 mixing ratios, which characterize the vortex in late fall, are already present at high latitudes at the end of summer in September before the vortex circulation sets up. The appearance of the seasonal minimum in O_3 is accompanied by an increase in zonal variance at the end of the summer. These features are also seen in a 3-D chemistry transport model (CTM) driven by meteorology from data assimilation. Analysis of the CTM output shows that the minimum O_3 and increase in variance in late summer are the result of 1) stirring of polar concentric O_3 gradients by nascent wave-driven transport, and 2) an acceleration of net photochemical loss as production via O2 photolysis slows faster than radical catalytic loss with decreasing solar illumination. The lowest O_3 amounts, generally at high latitudes, become isolated from mixing with lower latitude/higher O_3 air as the vortex strengthens. Continued chemical loss, increasing with altitude, contributes to the flattening of the vertical gradient and mixing within the vortex diminishes horizontal gradients in the vortex.

The seasonal time series also shows clearly the segregation of low O_3 mixing ratios into the vortex as the vortex circulation strengthens through the fall season. This suggests a possible feedback role between O_3 chemistry and the formation of the vortex, which is dominated by the seasonal radiation balance. Back trajectory calculations show that the air, which ultimately becomes the vortex in the middle stratosphere, originates almost exclusively at latitudes north of 67° in September, re-emphasizing the role of net radiative cooling. Forward trajectories from O_3

sample points early in fall show only a weak correlation between initial O_3 mixing ratio and PV later in the season. This indicates that, if there is a feedback between the chemistry that controls O_3 and the radiative processes that initiate vortex formation, it is subtle and difficult to detect with available data and techniques. This finding is consistent with order-of-magnitude calculations for the relative importance of O_3 in the fall radiative balance at high latitudes.

Similar characteristics are seen in most other years in the NH. We have looked at POAM III for 1998, which is quite similar to 1999 in November/December, and 2000 (Figure 5), POAM II for 1993 to 1996, and MLS data for earlier years. POAM does not always sample a range of PV that includes the vortex in November, but for those times with sampling at high equivalent latitudes, the distributions are similar to those presented here. We plan a follow-on study to examine the interannual variability of early winter O_3, vortex development, and vortex persistence and spring O_3 loss. A time series of O_3 at the South Pole [Cheng et al., 1997] shows a similar "flat" profile and a mixing ratio of about 3 ppmv in April consistent with POAM II and III data from the southern hemisphere. Waugh and Randel [1999] show that there is little interannual variability in the size of the vortex through the October/November formation period over 20 analyzed years, again emphasizing the radiative control of the early vortex stages. Manney and Sabutis [2000] found that the early vortex development in 1999 was dynamically similar in structure to other cold years in the NH (1994-1996), although late fall temperatures were colder than previous analyzed years.

The strong zonal asymmetry in the O_3 distribution at high latitudes has several implications. For one, it means that the zonal mean climatology may not be a good initial state for 3-D model

calculations during NH winter. The models should either be started early in the fall or should utilize a 3-D initial O_3 distribution. It also means that caution should be exercised in developing an initial state for O_3 loss calculations using a limited amount of data in the fall, e.g., from HALOE, which has limited high latitude sampling. Finally it suggests that a full 3-D O_3 field is needed for radiative calculations in general circulation models. We plan to run a test in the DAO model with 3D O_3 rather than the 2D climatology now used to see if the vortex develops more realistically.

The possible connection between O_3 chemistry and the dynamics of vortex formation suggests that these feedbacks and sensitivities need to be better understood. Initial (November) column O_3 at high latitudes is not well correlated with the minimum O_3 in spring (March); however, the strength of the vortex does exert a strong control on the amount of chemical O_3 loss in spring [Newman et al., 2001]. To the extent that the dynamics of the vortex is linked to the abundance of O_3, these processes and their interactions need to be well represented in order to make confident predictions of the recovery of NH O_3.

Acknowledgements:

The authors would like to acknowledge helpful conversations with L. W. Coy, P. A. Newman, J. E. Rosenfield, and D. W. Waugh. This work was supported as part of the SOLVE campaign by the NASA Upper Atmosphere Research Program and Atmospheric Chemistry Modeling and Analysis Program.

References:

Anderson, D. E., Jr., and S. A. Lloyd, Polar twilight UV-visible radiation field: perturbations due to multiple scattering, ozone depletion, stratospheric clouds, and surface albedo, *J. Geophys. Res., 95,* 7429-7434, 1990.

Baldwin, M. P., and J. R. Holton, Climatology of the stratospheric polar vortex and planetary wave breaking, *J. Atmos. Sci., 45*, 1123-1142, 1988.

Bowman, K. P., and A. J. Krueger, A global climatology of total ozone from the Nimbus 7 Total Ozone Mapping Spectrometer, *J. Geophys. Res., 90*, 7967-7976, 1985.

Bruhl, C., and P. J. Crutzen, NOx-catalyzed ozone destruction and NOx activation at midlatitudes to high latitudes as the main cause of the spring to fall ozone decline in the Northern Hemisphere, *J. Geophys. Res., 105*, 12,163-12,168, 2000.

Bruhl, C., P. J. Crutzen, J.-U. Groos, High latitude summertime NOx activation and seasonal ozone decline in the lower stratosphere: Model calculations based on observations by HALOE on UARS, J. Geophys. Res., 103, 3587-3597, 1998.

Butchart, N., and E. E. Remsberg, The area of the stratospheric polar vortex as a diagnostic for tracer transport on an isentropic surface, *J. Atmos. Sci., 43*, 1319-1339, 1986.

Clough, S. A., N. S. Grahame, A. O'Neill, Potential vorticity in the stratosphere derived using data from satellites, *Q. J. R. Meteorol. Soc., 111*, 335-358, 1985.

Cheng, D., S. Crewell, U. Klein, R. de Zafra, Millimeter wave spectroscopic measurements over the South Pole 4. O_3 and N_2O during 1995 and their correlations for two quasi-annual cycles, *J. Geophys. Res., 102*, 6109-6116, 1997.

Cordero, E. C. and S. R. Kawa, Ozone and tracer transport variations in the summer northern hemisphere stratosphere, *J. Geophys. Res., 106,* 12,227-12,239, 2001.

Douglass, A. R. and S. R. Kawa, Contrast between 1992 and 1997 high latitude spring Halogen Occultation Experiment observations of lower stratospheric HCl, *J. Geophys. Res.*, *104*, 18,739-18,754, 1999.

Douglass, A. R., M. R. Schoeberl, S. R. Kawa, E. V. Browell, A composite view of ozone evolution in the 1995-96 northern winter polar vortex developed from airborne lidar and satellite observations, *J. Geophys. Res., 106,* 9879-9895, 2001.

Fahey, D. W., and A. R. Ravishankara, Summer in the stratosphere, *Science, 285,* 208-210, 1999.

Farman, J. C., R. J. Murgatroyd, A. M. Silnickas, B. A. Thrush, Ozone photochemistry in the Antarctic stratosphere in summer, *Q. J. R. Meteorol. Soc., 111,* 1013-1028, 1985.

Fels, S. B., J. D. Mahlman, M. D. Schwarzkopf, et al., Stratospheric sensitivity to perturbations in ozone and carbon-dioxide - radiative and dynamical response, *J. Atmos. Sci., 37*, 2265-2297, 1980.

Froidevaux, L., J. W. Waters, W. G. Read, Global ozone observations from the UARS MLS - An overview of zonal-mean results, *J. Atmos. Sci., 51,* 2846-2866, 1994.

Hoppel, K. W., K. P. Bowman, R. M. Bevilacqua, Northern hemisphere summer ozone variability observed by POAM II, *Geophys. Res. Lett., 26,* 827-830, 1999.

JPL, Chemical kinetics and photochemical data for use in stratospheric modeling, Evaluation Number 12, DeMore, W.B., et al., eds., JPL Publication 97-4, 1997.

JPL, Chemical kinetics and photochemical data for use in stratospheric modeling, Evaluation Number 13, Sander, S. P., et al., eds., JPL Publication 00-3, 2000.

Juckes, M. N., and A. O'Neill, Early winter in the northern stratosphere, *Q. J. R. Meteorol. Soc., 114*, 1111-1125, 1988.

Kirk-Davidoff D. B., E. J. Hintsa, J. G. Anderson, D. W. Keith, The effect of climate change on ozone depletion through changes in stratospheric water vapour, *Nature, 402*, 399-401, 1999.

Labitzke, K., Interannual variability of the winter stratosphere in the northern hemisphere, *Mon. Wea. Rev., 105*, 762-770, 1977.

Labitzke, K., On the interannual variability of the middle stratosphere during the northern winter, *J. Meteorol. Soc. Japan, 60*, 124-138, 1982.

Lait, L. R., An alternative form for potential vorticity, *J. Atmos. Sci., 51*, 1754-1759, 1994.

Leovy, C. B., C. R. Sun, M. H. Hitchman, et al., Transport of ozone in the middle stratosphere - evidence for planetary wave breaking, *J. Atmos. Sci., 42*, 230-244, 1985.

Lin, S. J., and R. B. Rood, Multidimensional flux form semi-Lagrangian transport schemes, *Mon. Wea. Rev., 124,* 2046-2070, 1996.

Logan, J. A., and R. D. McPeters, Ozone Climatology, Chapter 4 in Models and Measurements II, ed. J. H. Park, M. K. W. Ko, C. H. Jackman, and R. A. Plumb, NASA/TM-1999-209554, 1999.

Lucke, R. L., et al., The Polar Ozone and Aerosol Measurement (POAM) III instrument and early validation results, *J. Geophys. Res., 104*, 18,785-18,799, 1999.

Lumpe, J. D., et al., Comparison of POAM III ozone measurements with correlative aircraft and balloon data during SOLVE, *J. Geophys. Res.*, in press, 2002.

Lumpe, J.D., R.M. Bevilacqua, K.W. Hoppel, and C.E. Randall, POAM III retrieval algorithm and error analysis, submitted to J. Geophys. Res., 2001]

Manney, G. L., L. Froidevaux, J. W. Waters, et al., Chemical depletion of ozone in the arctic - lower stratosphere during winter 1992-93, *Nature, 370*, 429-434, 1994.

Manney GL, Michelsen HA, Irion FW, et al., Lamination and polar vortex development in fall from ATMOS long-lived trace gases observed during November 1994, *J. Geophys. Res., 105*, 29023-29038, 2000.

Manney, G. L., and J. L. Sabutis, Development of the polar vortex in the 1999-2000 Arctic winter stratosphere, *Geophys. Res. Lett., 27*, 2589-2592, 2000.

Manney, G. L., H. A. Michelsen, M. L. Santee, et al., Polar vortex dynamics during spring and fall diagnosed using trace gas observations from the Atmospheric Trace Molecule Spectroscopy instrument, *J. Geophys. Res. 104*, 18841-18866, 1999.

Mueller R., P. J. Crutzen, J. U. Gross, et al., Severe chemical ozone loss in the Arctic during the winter of 1995-96, *Nature 389*, 709-712, 1997.

Nash, E.R., P. A. Newman, J. E. Rosenfield, M. R. Schoeberl, An objective determination of the polar vortex using Ertel's potential vorticity, *J. Geophys. Res., 10,* 9471-9478, 1996.

Newman, P. A., and N. R. P. Harris, An overview of the SOLVE-THESEO 2000 campaign, *J. Geophys. Res.,* in press, 2002.

Newman, P. A., D. W. Fahey, W. H. Brune, M. J. Kurylo, S. R. Kawa, Preface – Photochemistry of Ozone Loss in the Arctic Region in Summer, *J. Geophys. Res., 104*, 26,481-26,495, 1999.

Newman, P. A., E. R. Nash, and J. E. Rosenfield, What controls the temperature of the Arctic stratosphere during spring?, *J. Geophys. Res., 106,* 19,999-20,010, 2001.

O'Neill, A. and V. D. Pope, The seasonal evolution of the extra-tropical stratosphere in the southern and northern hemispheres: Systematic changes in potential vorticity and the non-conservative effects of radiation, in *Dynamics, Transport and Photochemistry I the*

Middle Atmosphere of the Southern Hemisphere, pp. 33-54, Kluwer Academic Publishers, 1990.

Park, J. H., J. M. Russell, III, Summer polar chemistry observations in the stratosphere made by HALOE, *J. Atmos. Sci., 51,* 2903-2913, 1994.

Perliski, L. M., S. Solomon, J. London, On the interpretation of seasonal variations of stratospheric ozone, *Planet. Space Sci., 37,* 1527-1538, 1989.

Ray et al

Rex, M., et al., Chemical loss of ozone for the winter of 1999-2000, J. Geophys. Res., in press, 2002.

Richard, E. C., K. C. Aikin, A. E. Andrews, B. C. Daube, Jr., C. Gerbig, S. C. Wofsy, P. A. Romashkin, D. F. Hurst, E. A. Ray, F. L. Moore, J. W. Elkins, T. Deshler, G. C. Toon, Severe chemical ozone loss inside the arctic polar vortex during winter 1999-2000 inferred from in-situ airborne measurements, *Geophys. Res. Lett., 28*, 2197-2200, 2001.

Rosenfield, J. E., Ozone, absorption and emission of radiation, in *Encyclopedia of Earth System Science*, Vol. *3*, 525-530, 1992.

Rosenlof, K. H., Estimates of the seasonal cycle of mass and ozone transport at high northern latitudes, *J. Geophys. Res., 104*, 26,511-26,523, 1999.

Rusch, D.W., C.E. Randall, R.M. Bevilacqua, K.W. Hoppel, E. Shettle, J.D. Lumpe, E Kyro, Validation of POAM III ozone: Comparisons with ozonesondes and satellite data, submitted to J. Geophys. Res., 2001.

Ruth S. L., J. J. Remedios, B. N. Lawrence, et al., Measurements of N2O by the UARS Improved Stratospheric and Mesospheric Sounder during the early northern winter 1991/92, *J. Atmos. Sci., 51*, 2818-2833, 1994.

Salawitch, R. J., et al., Chemical loss of ozone during the Arctic winter of 1999-2000: An analysis based on balloon-borne observations, J. Geophys. Res., in press, 2002.

Schoeberl, M. R., and D. L. Hartmann, The dynamics of the stratospheric polar vortex and its relation to springtime ozone depletions, *Science, 251*, 46-52, 1991.

Schoeberl, M. A., P. A. Newman, L. R. Lait, T. J. McGee, and J. F. Burris, E. V. Browell, W. B. Grant, E. C. Richard, P. von der Gathen, R. Bevilacqua, I. S. Mikkelsen, and M. J. Molyneux, An Assessment of the Ozone Loss During the 1999-2000 SOLVE/THESEO 2000 Arctic Campaign, *J. Geophys. Res., in press*, 2002.

Shindell, D. T., D. Rind, P. Lonergan, Increased polar stratospheric ozone losses and delayed eventual recovery owing to increasing greenhouse-gas concentrations, *Nature, 392,* 589-592, 1998.

Sinnhuber, B.-M., M. P. Chipperfield, S. Davies, J. P. Burrows, K.-U. Eichmann, M. Weber, P. von der Gathen, G. A. Cahill, A. M. Lee, J. A. Pyle, Large loss of total ozone during the Arctic winter of 1999/2000, *Geophys. Res. Lett., 27,* 3473-3476, 2000.

Stolarski, R. S., et al. 1995 scientific assessment of the atmospheric effects of stratospheric aircraft, *NASA Ref. Publ. 1381,* 1995.

Toon, G. C., et al., Comparison of MkIV balloon and ER-2 aircraft measurements of atmospheric trace gases, *J. Geophys., Res., 104*, 26,779-26,790, 1999.

WMO, Scientific Assessment of Ozone Depletion: 1998, *World Meteorological Organization Global Ozone Research and Monitoring Project, Report No. 44*, 1999.

Waugh, D. W., and W. J. Randel, Climatology of Arctic and Antarctic polar vortices using elliptical diagnostics, *J. Atmos. Sci, 56,* 1594-1613, 1999.

Figure Captions:

Figure 1. O_3 profiles from OMS data on November 11, 1999 (red), nearby POAM samples on November 17 and 20 (blue), and November climatology (black). Also shown are the PV distributions [Lait, 1994] at potential temperatures of 500, 650, and 800 K on November 19 from United Kingdom Meteorological Office analyzed data. The estimated boundary of the vortex [Nash et al., 1996] is shown by the white contour and the O_3 sample locations are shown for OMS (white) and POAM (blue symbols). Both ascent and descent profiles are shown for OMS. OMS O_3 data are taken every second with an overall uncertainty (precision and accuracy) of 3 to 5% [Salawitch et al., 2002].

Figure 2. O_3 profiles from POAM and PV distributions for November 30, 1999. O_3 profiles are color coded by their PV value at 650 K. POAM sample locations are shown by the white symbols on the PV maps.

Figure 3. Potential temperature-equivalent latitude composites of POAM O_3 data for the second half of November 1999. Data are interpolated to potential temperatures surfaces, and averages, standard deviations, and numbers of observations are calculated for each 5° equivalent latitude interval. The average position of the vortex edge [Nash et al., 1996] is shown by the dashed white line.

Figure 4. O_3 profiles from POAM and PV distributions for September 15, 1999. O_3 profiles are color coded by their PV value at 650 K. POAM sample locations are shown by the white symbols on the PV maps. Other days in mid-September are similar.

Figure 5. Time series of POAM III O_3 data from April 1998 through December 2000 interpolated to 650 K potential temperature. Sample latitudes are given above the upper axis.

Figure 6. Expanded view of part of POAM III O_3 time series shown in Figure 5. Symbols are color coded by potential vorticity at 650 K. Sample latitudes are shown across the top of the plot.

Figure 7. Time series of O_3 from the CTM interpolated to 650 K potential temperature and color coded by PV similar to Figure 6. Plots are shown at 4 different latitudes output once per day from the model.

Figure 8. Contour maps of O_3 mixing ratio at 3 potential temperature surfaces on August 15 and September 15, 1999 from the CTM. The POAM III sample latitude is near 60° and 68° N, respectively.

Figure 9. Time-latitude zonal mean distributions of net photochemical O_3 production in percent per month from the CTM. Red to brown colors denote net production and yellow to blue are net destruction. The zero contour line is bold. Production and loss rates for O_3 are calculated off line for each chemical cycle from the daily model output radical abundances. These compare

very closely to total production and loss saved during the model run. To the extent that constituent distributions are zonally symmetric, the zonal mean rates may be interpreted as representing a diel average at any point.

Figure 10. Zonally averaged short-wave heating and (negative) long-wave cooling rates from the meteorological assimilation underlying the CTM transport winds and temperatures. Values are given at 3 pressure levels, which correspond approximately to 500-800 K, for October 1, 1999.

Figure 11. Results from 75-day diabatic back trajectory simulation for November 30, 1999. The trajectory model of Schoeberl et al. [2002] is used with data from UKMO. Panel (a) shows the PV distribution and equal-area distribution of starting parcel positions. Panel (b) shows the location of the parcels on September 16, 1999 superimposed on a color-coded latitude background. The white parcel symbols are those from inside the vortex edge on November 15 in panel (a). The white circle marks the POAM sampling latitude in mid September. Panel (c) shows the beginning-in-time potential temperatures mapped onto the parcel positions on November 15. Panel (d) shows the beginning-in-time latitudes of the parcels mapped to November 15.

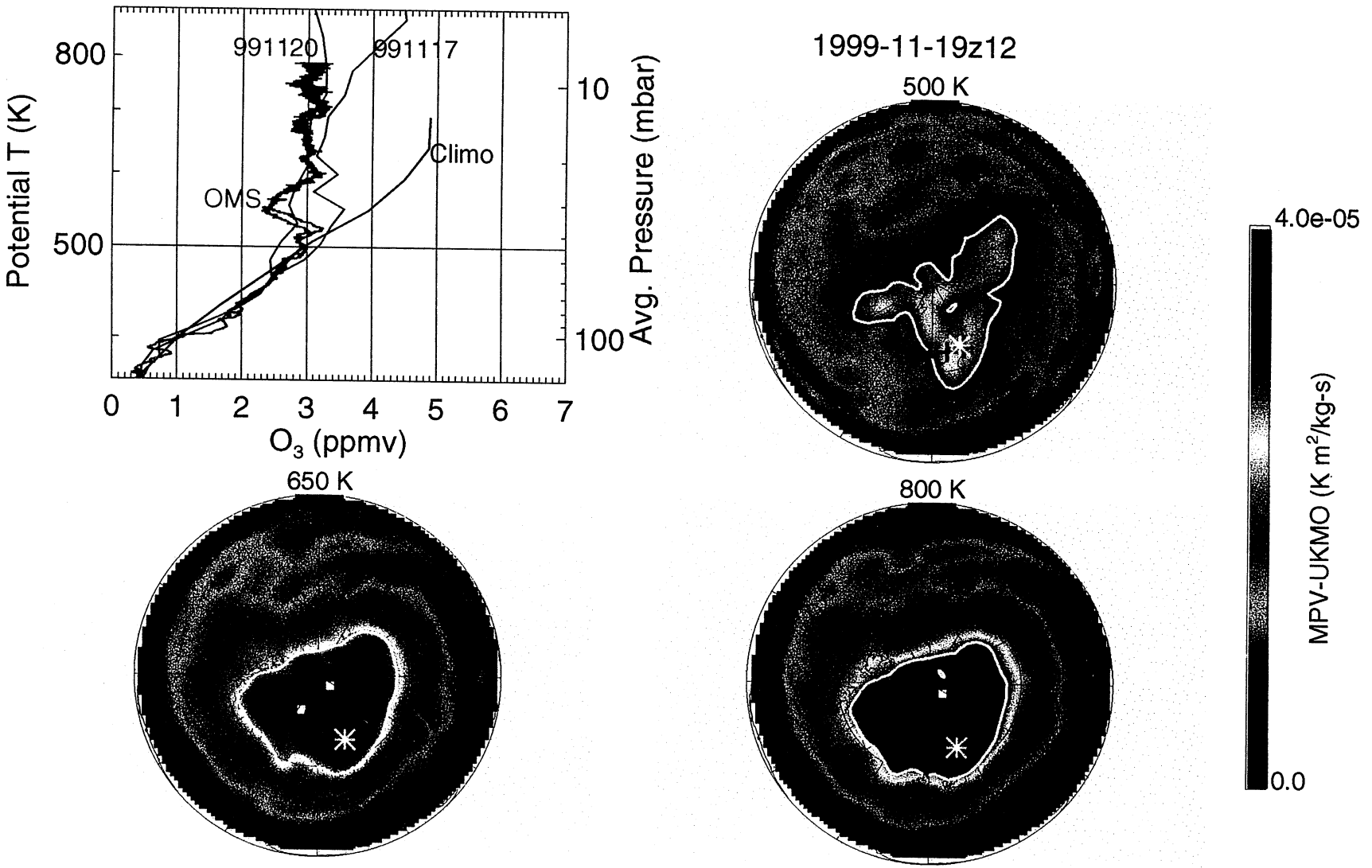
991120
991117
Climo
OMS
800
500
10
100
Potential T (K)
Avg. Pressure (mbar)
0 1 2 3 4 5 6 7
O_3 (ppmv)
650 K
1999-11-19z12
500 K
800 K
4.0e-05
0.0
MPV-UKMO (K m^2/kg-s)

Figure 1

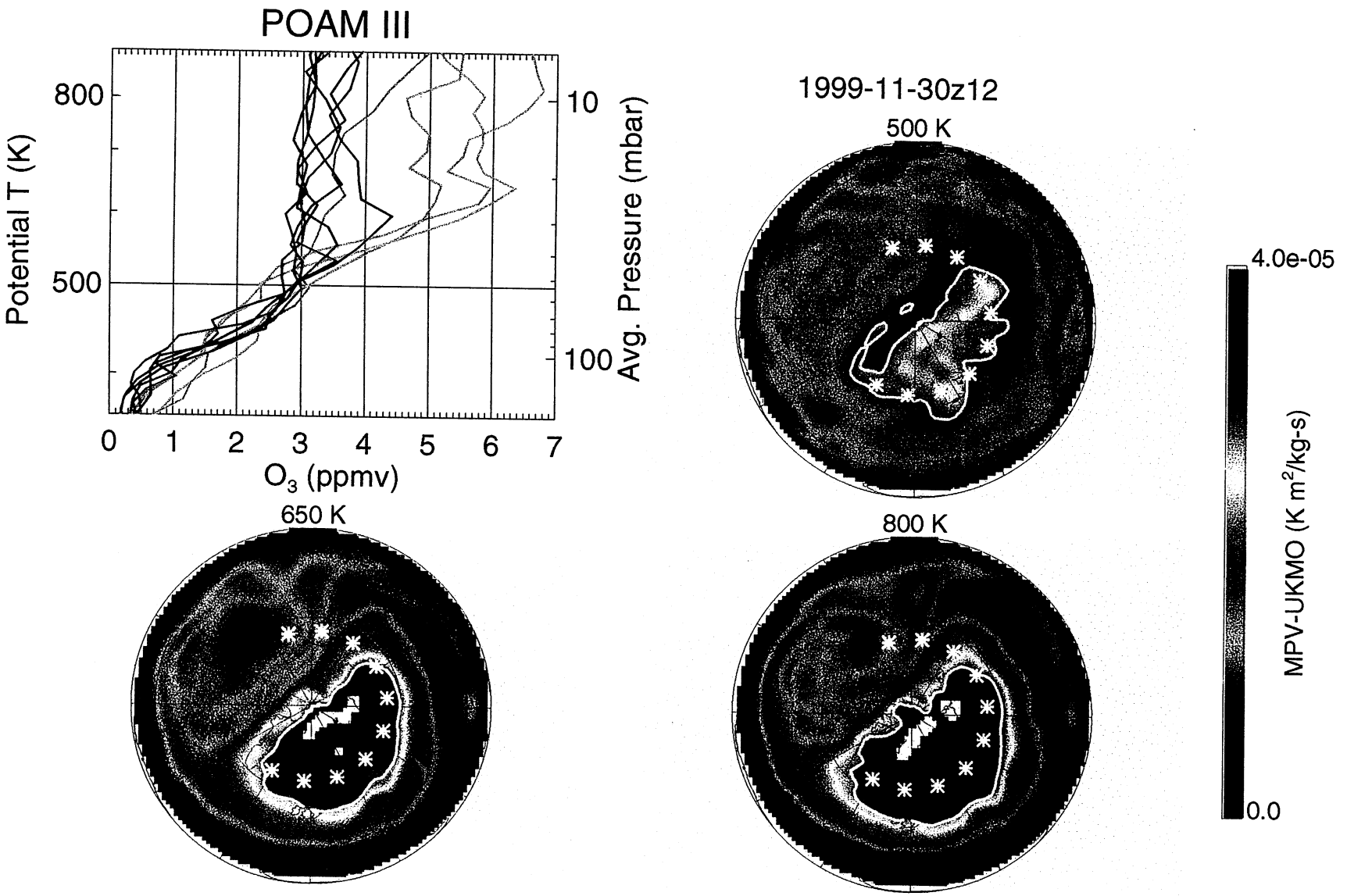
POAM III
Potential T (K)
800
500
10
100
Avg. Pressure (mbar)
0 1 2 3 4 5 6 7
O_3 (ppmv)
650 K
1999-11-30z12
500 K
800 K
4.0e-05
0.0
MPV-UKMO (K m^2/kg-s)

Figure 2

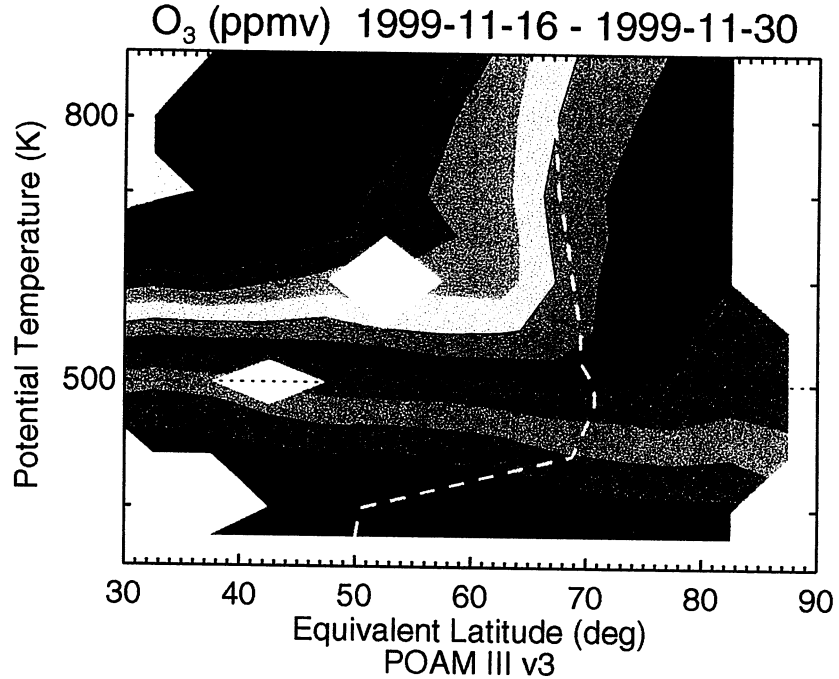
O_3 (ppmv) 1999-11-16 - 1999-11-30
Potential Temperature (K)
800
500
30
40
50
60
70
80
90
Equivalent Latitude (deg)
POAM III v3

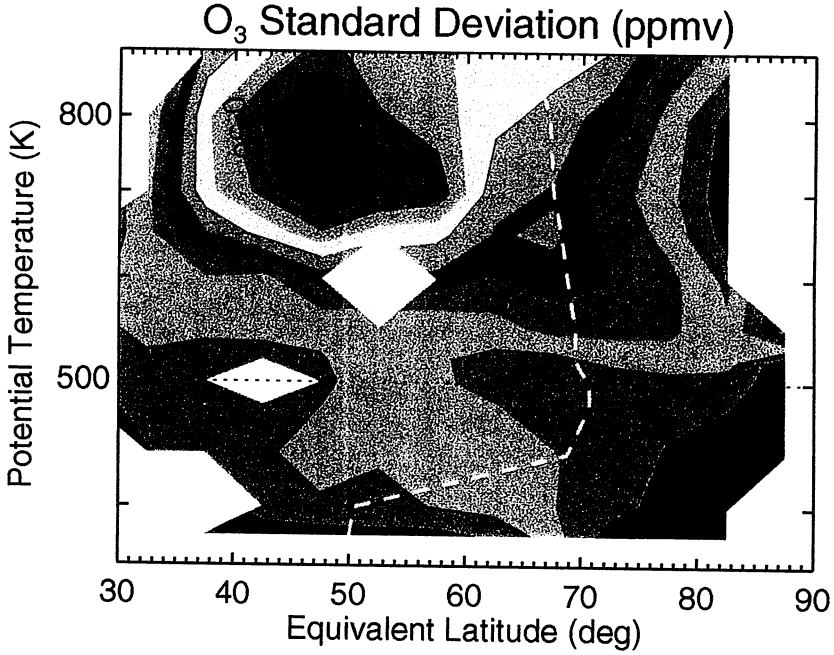
O_3 Standard Deviation (ppmv)
Potential Temperature (K)
800
500
30
40
50
60
70
80
90
Equivalent Latitude (deg)

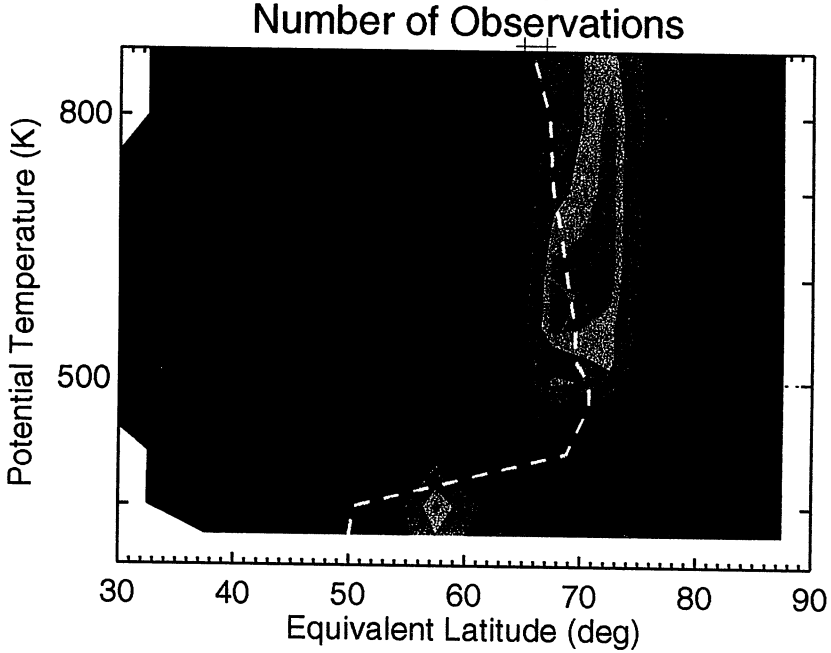
Number of Observations
Potential Temperature (K)
800
500
30
40
50
60
70
80
90
Equivalent Latitude (deg)

Figure 3

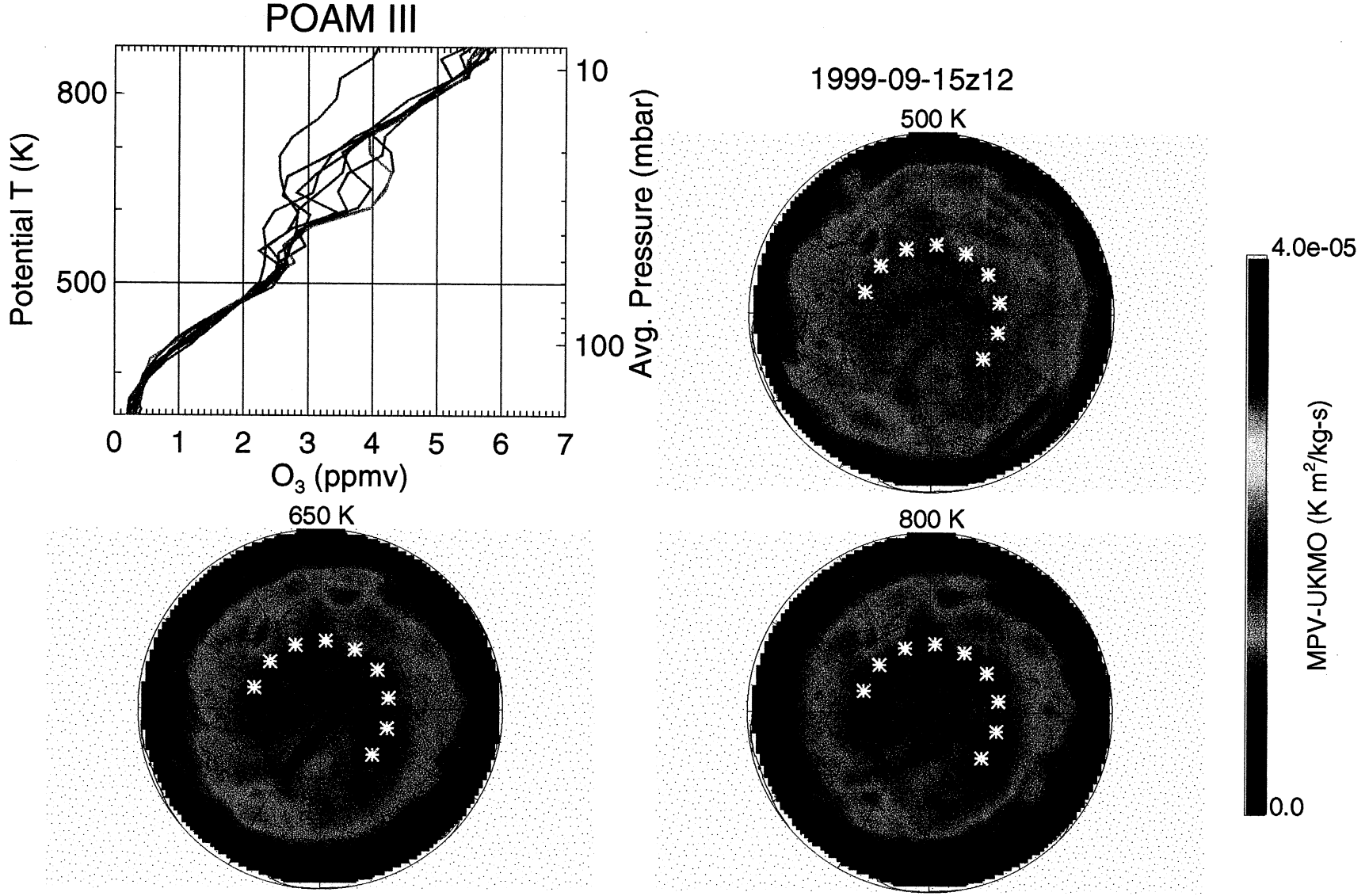
POAM III
Potential T (K)
800
500
0
1
2
3
4
5
6
7
O_3 (ppmv)
10
100
Avg. Pressure (mbar)
1999-09-15z12
500 K
650 K
800 K
4.0e-05
0.0
MPV-UKMO (K m^2/kg-s)

Figure 4

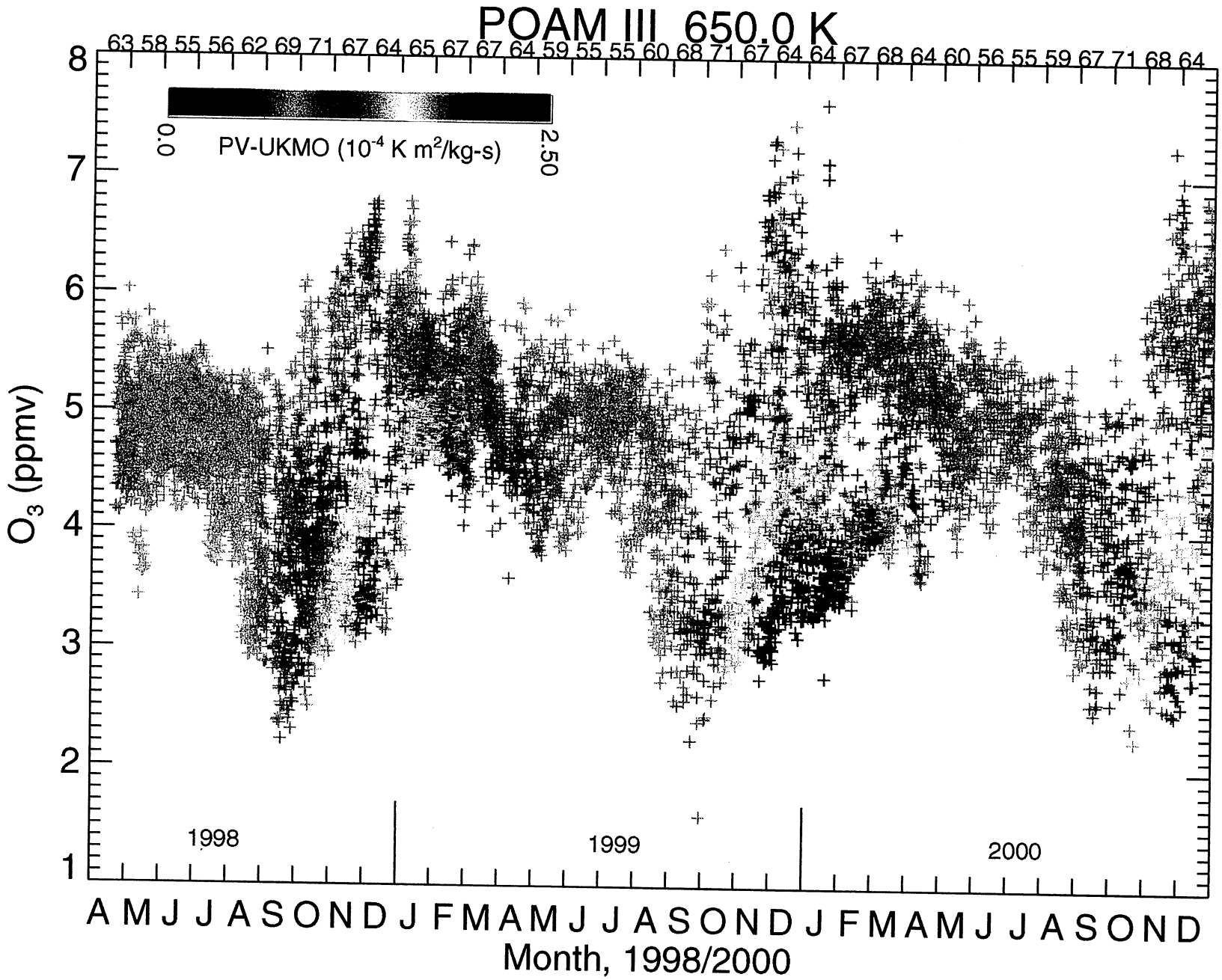
POAM III 650.0 K
63 58 55 56 62 69 71 67 64 65 67 67 64 59 55 55 60 68 71 67 64 64 67 68 64 60 56 55 59 67 71 68 64
0.0
PV-UKMO (10^{-4} K m^2/kg-s)
2.50
O_3 (ppmv)
1
2
3
4
5
6
7
8
1998
1999
2000
A M J J A S O N D J F M A M J J A S O N D J F M A M J J A S O N D
Month, 1998/2000

Figure 5

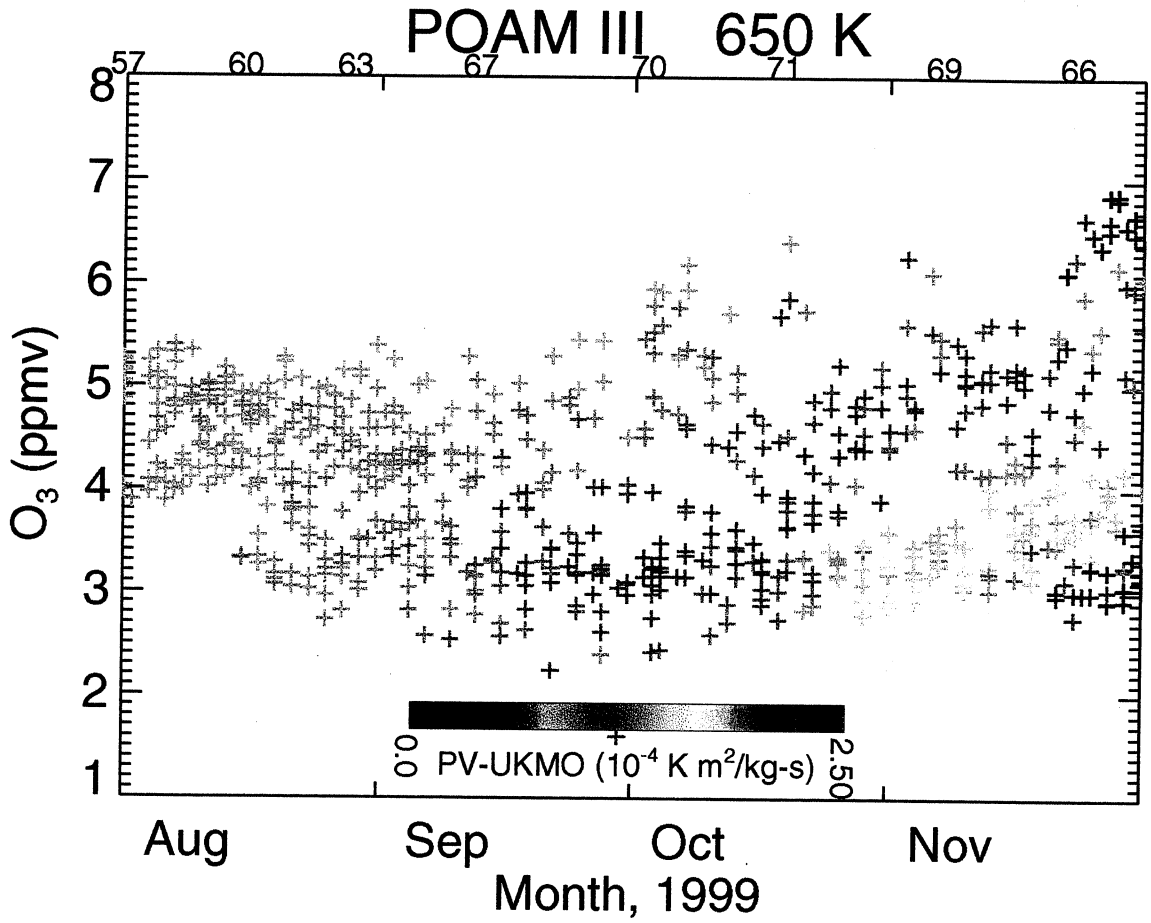
POAM III 650 K
57
60
63
67
70
71
69
66
8
7
6
5
4
3
2
1
O_3 (ppmv)
0.0
PV-UKMO (10^{-4} K m^2/kg-s)
2.50
Aug
Sep
Oct
Nov
Month, 1999

Figure 6

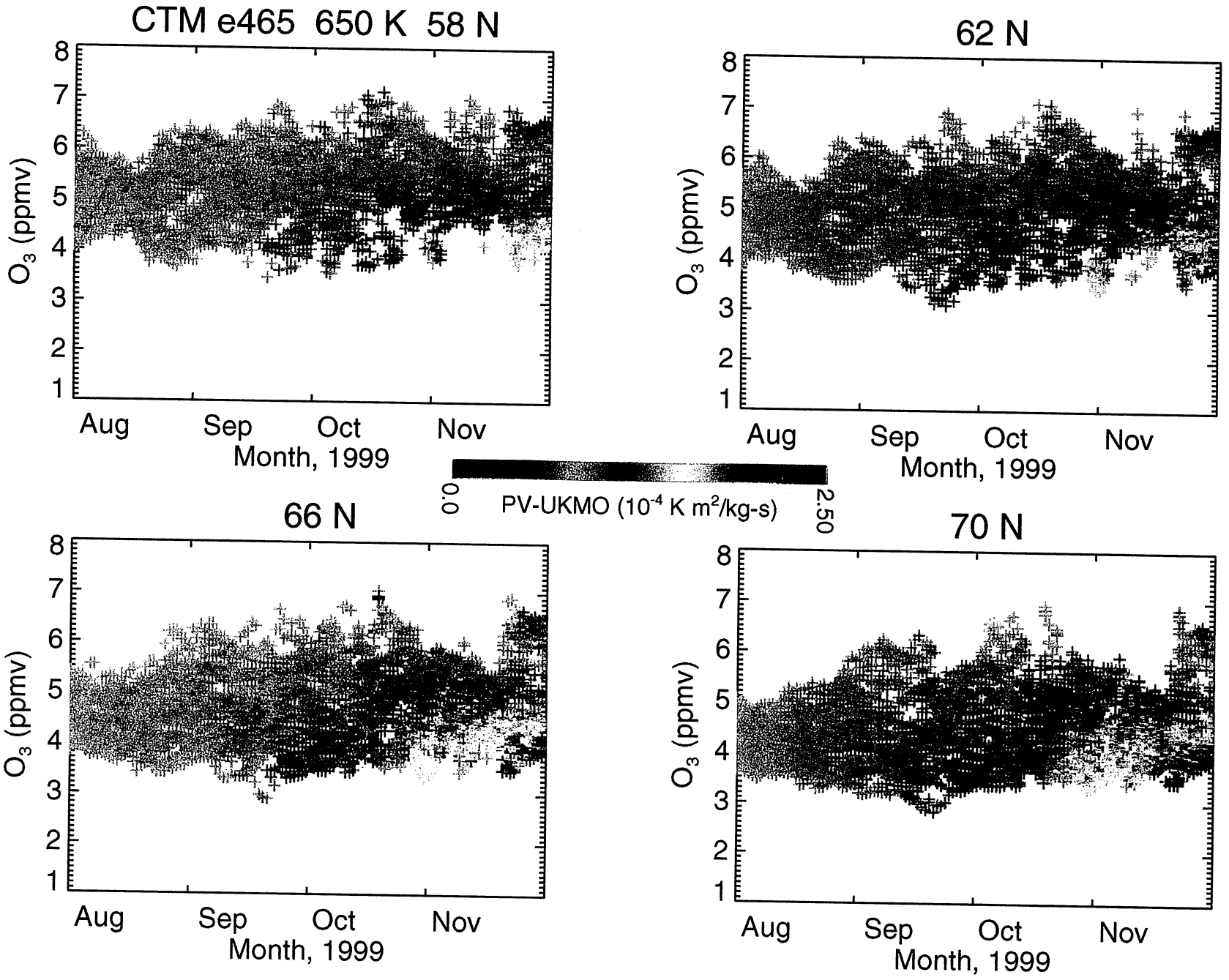
CTM e465 650 K 58 N
62 N
66 N
70 N
O_3 (ppmv)
Aug
Sep
Oct
Nov
Month, 1999
0.0
2.50
PV-UKMO (10^{-4} K m^2/kg-s)

Figure 7

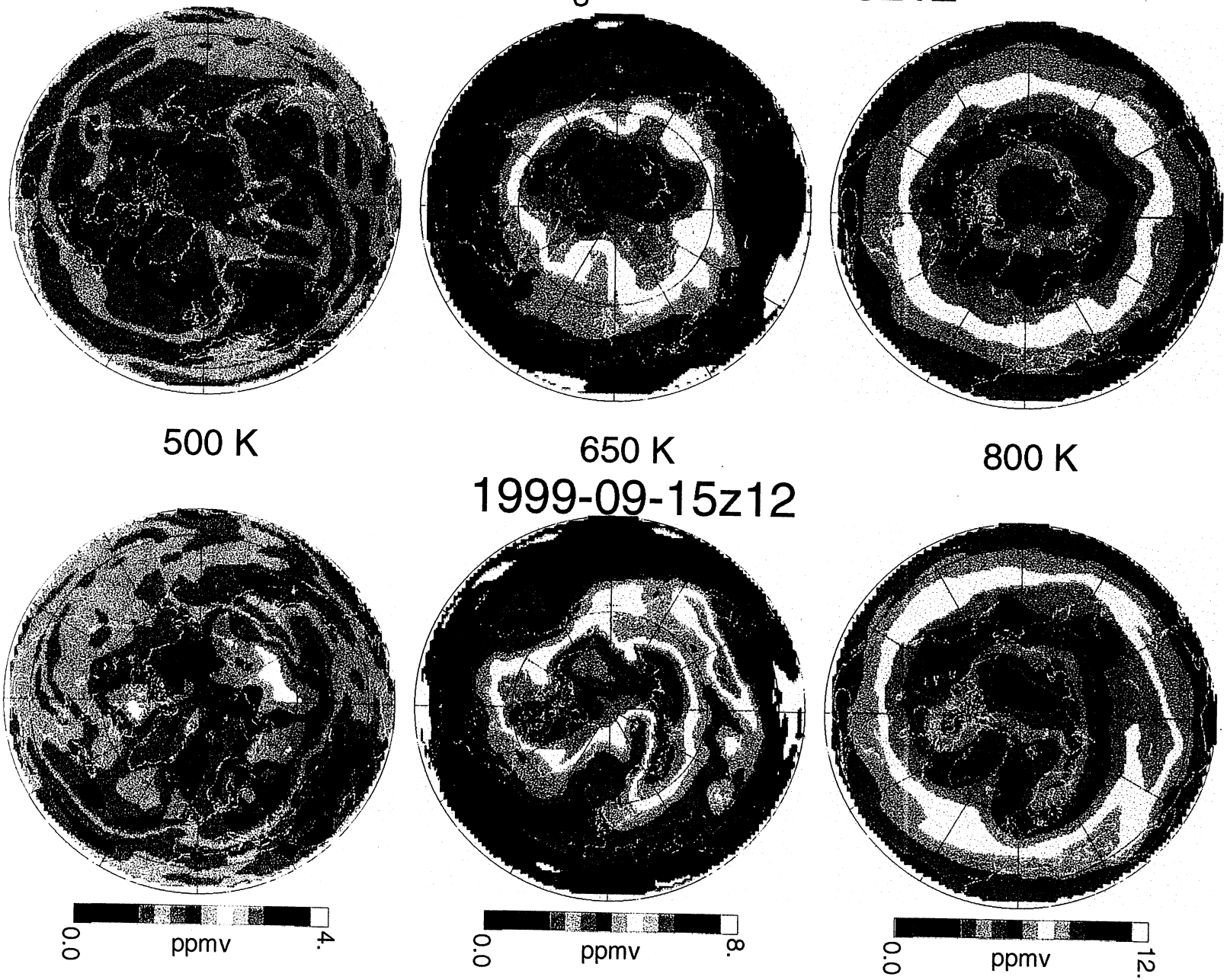
CTM e465 O_3 1999-08-15z12
500 K
650 K
800 K
1999-09-15z12
0.0
ppmv
4.
0.0
ppmv
8.
0.0
ppmv
12.

Figure 8

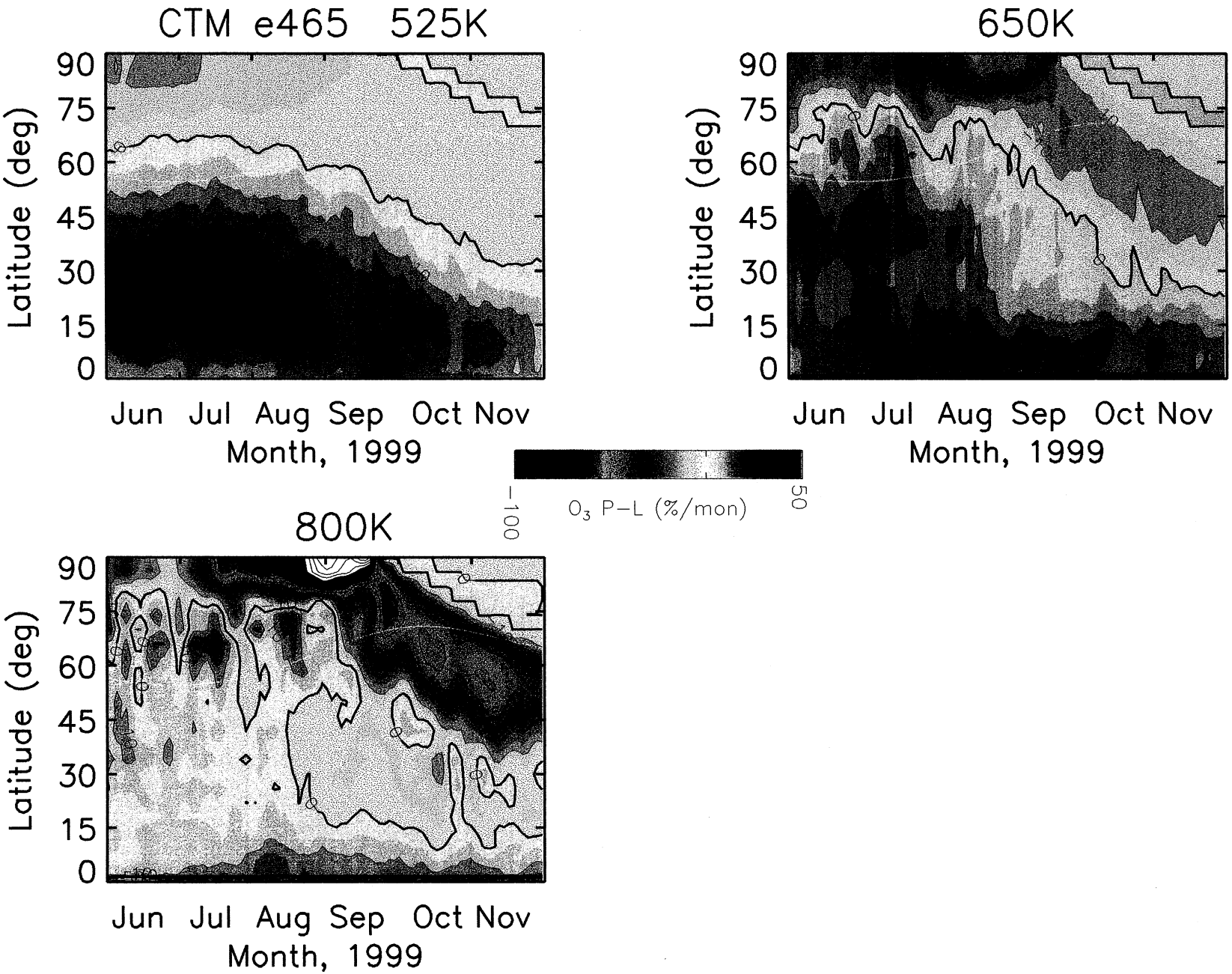
CTM e465 525K
650K
800K
Latitude (deg)
90
75
60
45
30
15
0
Jun Jul Aug Sep Oct Nov
Month, 1999
−100
50
O3 P−L (%/mon)

Figure 9

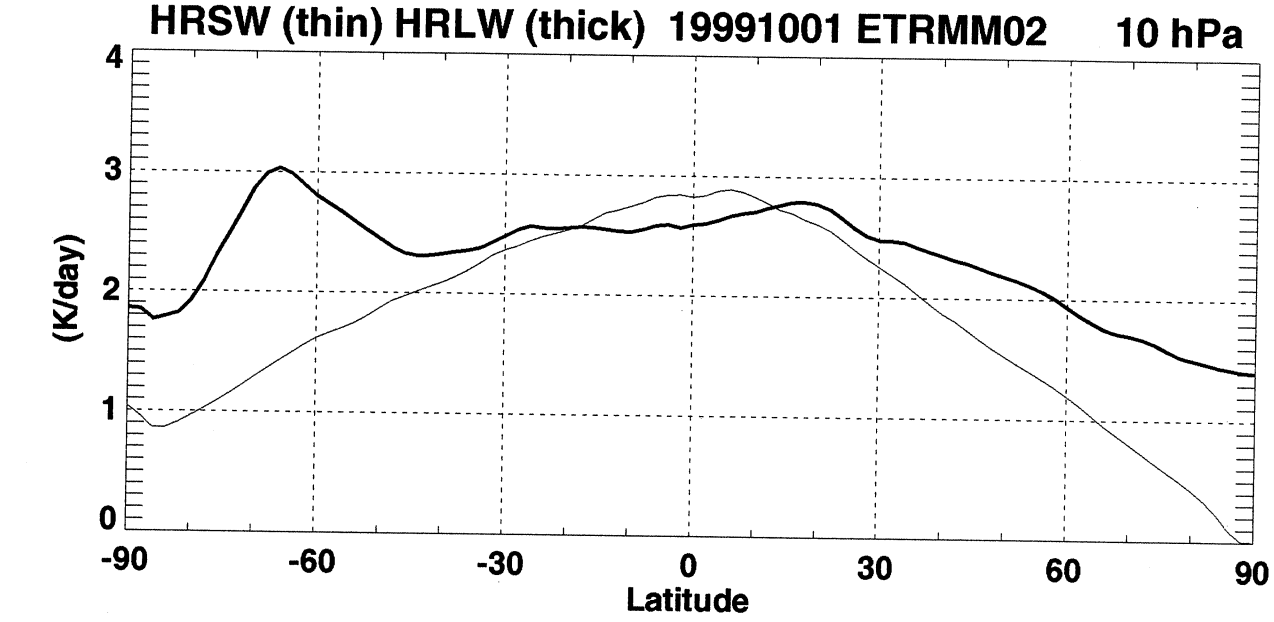
HRSW (thin) HRLW (thick) 19991001 ETRMM02 10 hPa
(K/day)
4
3
2
1
0
-90
-60
-30
0
30
60
90
Latitude

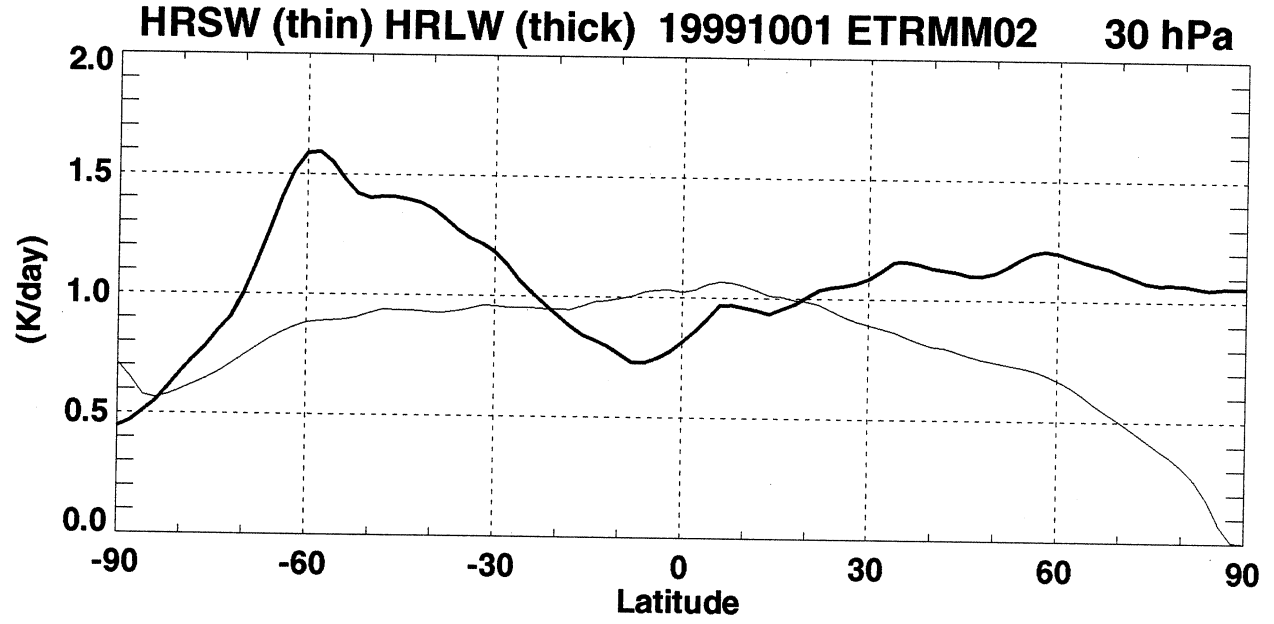
HRSW (thin) HRLW (thick) 19991001 ETRMM02 30 hPa
(K/day)
2.0
1.5
1.0
0.5
0.0
-90
-60
-30
0
30
60
90
Latitude

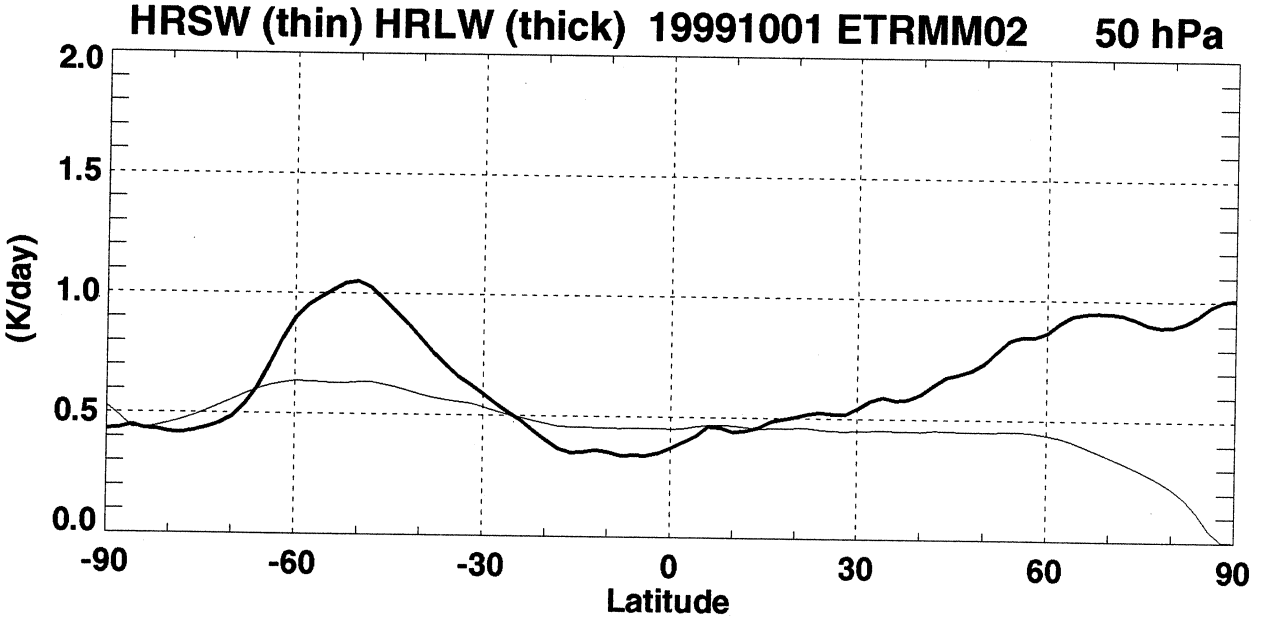
HRSW (thin) HRLW (thick) 19991001 ETRMM02 50 hPa
(K/day)
2.0
1.5
1.0
0.5
0.0
-90
-60
-30
0
30
60
90
Latitude

Figure 10

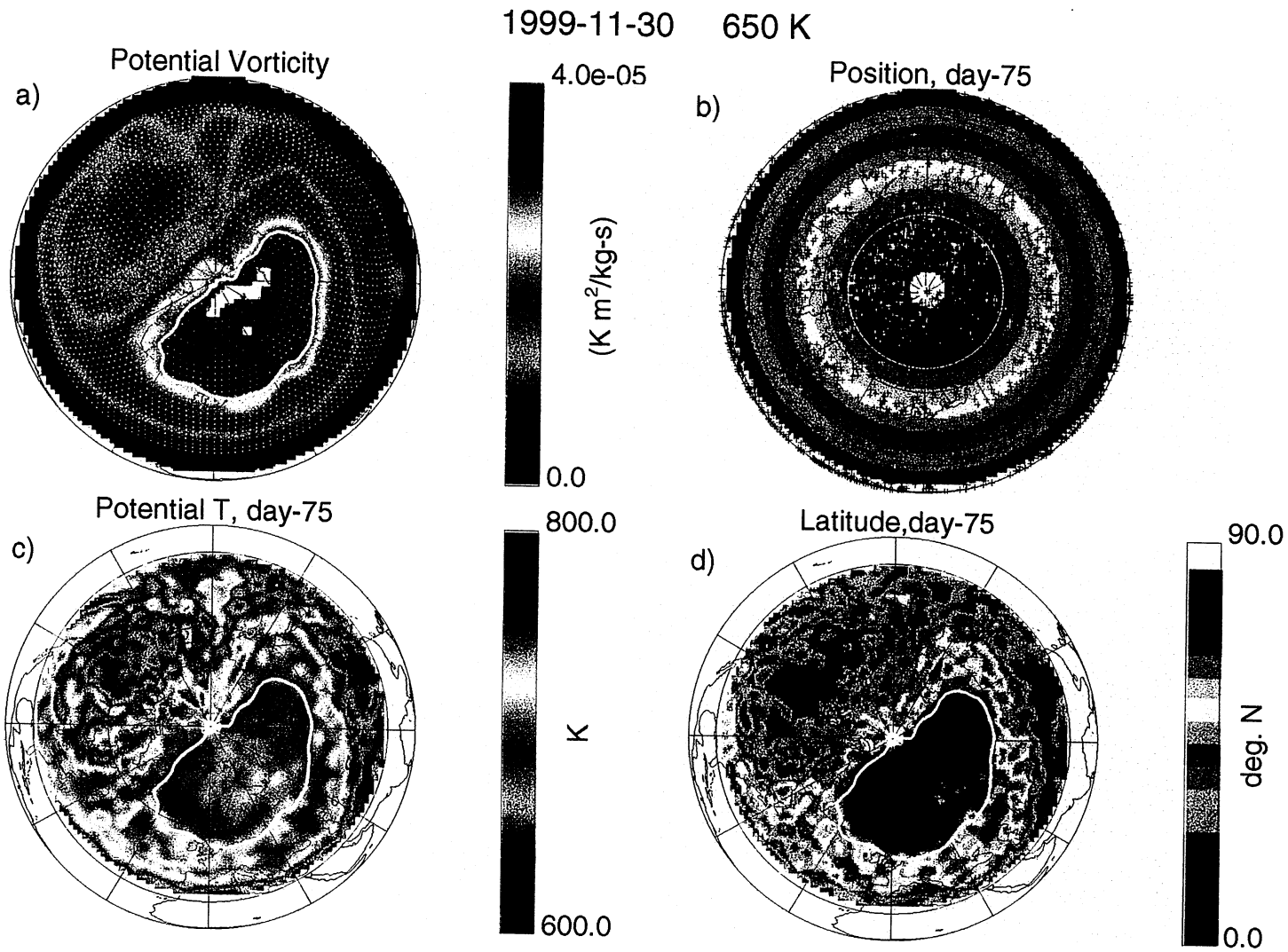
1999-11-30 650 K
Potential Vorticity
a)
4.0e-05
0.0
(K m²/kg-s)
Position, day-75
b)
Potential T, day-75
c)
800.0
600.0
K
Latitude,day-75
d)
90.0
0.0
deg. N

Figure 11

POPULAR SUMMARY

In this paper the morphology and evolution of the stratospheric ozone (O_3) distribution at high latitudes during the late summer and fall seasons are explored in the context of the SOLVE/THESEO field mission performed during winter 1999-2000. Unusual behavior of O_3 is observed, and the causes and reasons behind the peculiar behavior are explained using in situ and satellite data along with a three-dimensional model of chemistry and transport (CTM). O_3 in the vortex at the beginning of the winter season is found to be nearly constant from 500 to above 800 K with a value at 3 ppmv (+/- ~10%), which is very different from zonal mean climatology. Values outside the vortex are up to a factor of 2 higher and increase significantly with potential temperature. Analysis of data from the Polar Ozone and Aerosol Measurement satellite and the CTM shows that the low O_3 and large variance begin in late summer as the result of 1) stirring of polar concentric O_3 gradients by nascent wave-driven transport, and 2) an acceleration of net photochemical loss with decreasing solar illumination. Segregation of low O_3 mixing ratios into the vortex suggests a possible feedback role between O_3 chemistry and the vortex formation dynamics, which may need to be better understood in order to make confident predictions of the recovery of NH O_3.